

Laminar differences in the spatiotemporal structure of simple cell receptive fields in cat area 17

A. MURTHY,¹ A.L. HUMPHREY,^{1,2} A.B. SAUL,¹ AND J.C. FEIDLER^{1,2}

¹Department of Neurobiology, University of Pittsburgh School of Medicine, Pittsburgh, PA

²Center for the Neural Basis of Cognition, Pittsburgh

(RECEIVED May 8, 1997; ACCEPTED September 11, 1997)

Abstract

Previous studies of cat visual cortex have shown that the spatiotemporal (S-T) structure of simple cell receptive fields correlates with direction selectivity. However, great heterogeneity exists in the relationship and this has implications for models. Here we report a laminar basis for some of the heterogeneity. S-T structure and direction selectivity were measured in 101 cells using stationary counterphasing and drifting gratings, respectively. Two procedures were used to assess S-T structure and its relation to direction selectivity. In the first, the S-T orientations of receptive fields were quantified by fitting response temporal phase versus stimulus spatial phase data. In the second procedure, conventional linear predictions of direction selectivity were computed from the amplitudes and phases of responses to stationary gratings. Extracellular recording locations were reconstructed histologically. Among direction-selective cells, S-T orientation was greatest in layer 4B and it correlated well ($r = 0.76$) with direction selectivity. In layer 6, S-T orientation was uniformly low, overlapping little with layer 4B, and it was not correlated with directional tuning. Layer 4A was intermediate in S-T orientation and its relation ($r = 0.46$) to direction selectivity. The same laminar patterns were observed using conventional linear predictions. The patterns do not reflect laminar differences in direction selectivity since the layers were equivalent in directional tuning. We also evaluated a model of linear spatiotemporal summation followed by a static nonlinear amplification (exponent model) to account for direction selectivity. The values of the exponents were estimated from differences between linearly predicted and actual amplitude modulations to counterphasing gratings. Comparing these exponents with another exponent—that required to obtain perfect matches between linearly predicted and measured directional tuning—indicates that an exponent model largely accounts for direction selectivity in most cells in layer 4, particularly layer 4B, but not in layer 6. Dynamic nonlinearities seem essential for cells in layer 6. We suggest that these laminar differences may partly reflect the differential involvement of geniculocortical and intracortical mechanisms.

Keywords: Visual cortex, Direction selectivity, Receptive fields, Response timing, Linear summation, Nonlinear responses, Laminar location

Introduction

Many simple cells in cat visual cortex possess spatiotemporally (S-T) oriented receptive fields, which are characterized by a gradual progression of response timing across the receptive field (Movshon et al., 1978; Reid et al., 1987; McLean & Palmer, 1989; Albrecht & Geisler, 1991; Saul & Humphrey, 1992a). The significance of S-T orientation is that it can confer a preferred direction of stimulus motion. An object moving in a direction that successively activates receptive-field positions with progressively shorter latencies will elicit a strong net response due to coincident acti-

vation. Motion in the opposite direction will elicit less temporal coincidence and a weaker net response.

A model of linear summation within an S-T oriented receptive field has been successful in accounting for some of the directional properties in simple cells. S-T structure almost always predicts a cell's preferred direction of motion and it accounts for some of its directional tuning (Reid et al., 1991). However, the relationship between direction selectivity and S-T structure is highly variable. For some cells S-T structure accounts for most of the directional tuning whereas for others it accounts for almost none (Reid et al., 1991). In addition, the correlation between the two measures varies widely among studies, from ~ 0.7 (Albrecht & Geisler, 1991) to ~ 0.2 (Tolhurst & Dean, 1991).

The discrepancies between linear predictions and actual direction selectivity imply a role for nonlinear mechanisms. Albrecht and Geisler (1991) showed that a static nonlinearity such as that

Correspondence and reprint requests to: Allen Humphrey, Department of Neurobiology, E1440 Biomedical Science Tower, University of Pittsburgh School of Medicine, Pittsburgh, PA 15261, USA.

revealed in contrast-response functions improves predictions. The nonlinearity takes the form of a power-law amplification of response biases that are created initially by S-T oriented receptive-field structure. This type of model is referred to as an LN model, and consists of a linear, or first-order space-time filter followed by static nonlinearities. An alternative set of models (Emerson & Citron, 1992) specifies most of the directional tuning as resulting from dynamic nonlinearities, which influence response timing. Evidence for these alternative models comes from stimulation techniques that reveal second-order space-time interactions in receptive fields that account substantially for directional tuning in simple cells that lack first-order S-T orientation (Emerson & Citron, 1989; Baker & Boulton, 1994).

These observations indicate that a variety of mechanisms underlie direction selectivity. For some cells linear and static nonlinear processes may play a dominant role whereas for others dynamic nonlinearities may be critical. However, as yet no patterns of organization have been observed that might suggest rules for the application of these operations.

In area 17, simple cells reside primarily in two different layers, 4 and 6, with layer 4 receiving the bulk of input from the lateral geniculate nucleus. Since previous studies of S-T structure generally were not concerned with the laminae in which cells were recorded, we wondered whether some of the heterogeneity in S-T structure might be attributable to laminar location. Thus, we re-examined first-order S-T structure and direction selectivity in simple cells as a function of cortical layer. Our approach was similar to previous studies in that responses to counterphasing gratings were used to characterize S-T structure and to estimate the linear contribution to direction selectivity. Unlike most previous studies, which used both the amplitude and temporal phase of responses to counterphasing gratings to make linear predictions, we relied primarily on response phase (i.e. timing). The rationale for this is that the organization of response phase across the receptive field (i.e. S-T orientation) is key to understanding directional tuning in most simple cells. In contrast, response amplitude is distorted by static nonlinearities, and this tends to produce underestimates of the linear component of direction selectivity (Albrecht & Geisler, 1991; Heeger, 1993). By definition, response phase is not affected by static nonlinearities. In the experimental paradigm used here, response phase is sufficient to make linear predictions. We developed a new method for quantifying S-T orientation, based only on response phase, and we used the resulting metric to explore the contributions of linear and nonlinear mechanisms to direction selectivity.

We found that laminar differences do exist among simple cells in the relationship between S-T structure and directional tuning. Receptive fields of cells in lower layer 4 display the greatest degree of S-T orientation and the strongest correlation with direction selectivity. Cells in layer 6, in contrast, display little or no S-T orientation despite being direction selective. These findings can account partially for the previously observed heterogeneity in S-T structure of direction-selective cells. We also examined the ability of an LN model to account for directional tuning. For most cells in layer 4 direction selectivity can be explained adequately by this model. However, it does not account for the tuning of layer 6 cells or a few layer 4 cells. Dynamic nonlinearities seem to be essential for those cells. These findings suggest that the contributions that various mechanisms make to direction selectivity vary across cortical layers.

Portions of these results were reported in abstract form (Murthy et al., 1997).

Methods

Physiological preparation

Adult cats were prepared as previously described in detail (Humphrey et al., 1985; Saul & Humphrey, 1990). Anesthesia was induced using 4% halothane in nitrous oxide (70%) and oxygen (30%) and maintained during subsequent surgery using 1–2% halothane in the gas mixture. Cannulations of the radial vein and femoral artery were performed for delivering drugs and monitoring blood pressure, respectively. A tracheostomy was performed and the animal was ventilated at a rate sufficient to maintain end-tidal CO₂ at 4%. Rectal temperature was maintained at 37.5° C. Paralysis was maintained during recording using a continuous infusion of gallamine triethiodide (Sigma Chemical Co., St. Louis, MO; 5 mg·kg⁻¹·h⁻¹) and d-tubocurarine chloride (Sigma; 0.35 mg·kg⁻¹·h⁻¹) in 6 ml/h of 5% dextrose and lactated Ringer's solution. Additional lactated Ringer's solution was infused at 5–10 ml/h to stabilize blood pressure and maintain hydration.

Care was taken to ensure proper anesthesia during the experiment. Lidocaine HCl (2%) was applied to all incisions and pressure points. The head was supported nontraumatically in the stereotaxic by a crossbar attached to screws inserted into the skull. This permitted removal of the ear and eye bars. Heart rate and mean arterial blood pressure were monitored continuously to assess physiological state. Blood pressure was maintained at ~100 mm Hg. The raw and Fourier-analyzed cortical electroencephalogram (EEG) were monitored and the halothane level was adjusted to maintain the dominant frequencies of the EEG below 4 Hz during all stages of the experiment.

The pupils were dilated with atropine and the corneas were covered with contact lenses fitted with 3-mm artificial pupils. Refraction was evaluated by slit retinoscopy and contact lenses were chosen to focus the eyes at 57 cm.

Recording, visual stimulation, and cell classification

Extracellular recordings of single neurons were made using micropipettes filled with 0.2 to 2 M KCl (~80 to 35 MΩ, respectively). Signals were amplified, displayed on an oscilloscope, and fed to an audio monitor and a window discriminator. Action potentials were converted to pulses with 1-ms accuracy.

Receptive fields were plotted initially on a tangent screen using a hand-held ophthalmoscope. All subsequent stimuli were presented at 57 cm from the eyes on a Tektronix 608 monitor driven by a Picasso image synthesizer (Innisfree, Cambridge, MA) linked to an LSI-11/73 computer. The monitor subtended ~10 deg of visual angle. Stimuli were presented monocularly with the non-dominant eye occluded. Mean luminance was 15 cd/m² and Rayleigh-Michaelson contrast was ~40%.

Preferred values of stimulus orientation and spatial and temporal frequency were determined for each cell using drifting sine-wave gratings. These values were then used during subsequent testing. Drifting and counterphasing sine-wave gratings were used to measure direction selectivity and S-T receptive-field structure, respectively. The spatial phase of the counterphasing grating was varied over one-half cycle of the stimulus spatial frequency to test 8 or 16 phases. Each spatial phase was presented for 3–5 trials, or more if responses were noisy and more averaging was required. Each direction of the drifting grating was presented 12–20 times. All stimuli were randomly interleaved. Each trial usually lasted 4 s, with a 1-s intertrial interval of uniform screen luminance.

Simple cells were identified by the presence of distinct spatially offset ON and OFF flanks in the receptive field (Hubel & Wiesel, 1962), and modulated responses to sine-wave stimuli (Skottun et al., 1991). Modulation was quantified as the ratio of the first harmonic amplitude to the DC component in response to a grating drifting in the preferred direction. Simple cells had ratios greater than 1.

Data analysis

Action potentials were summed into peristimulus time histograms (PSTHs) to measure the average response per cycle of the periodic stimulus. Each PSTH was Fourier analyzed to obtain the first harmonic response amplitude and temporal phase. Response phase is expressed in cycles relative to the stimulus.

Responses to drifting gratings were used to compute a directional index (*DI*) given by

$$DI = (PD - NPD)/(PD + NPD) \quad (1)$$

where, *PD* and *NPD* are the response amplitudes in the preferred and nonpreferred directions of motion, respectively. The index varies from 0 to 1, signifying no or complete direction selectivity, respectively. Only cells with *DI*s greater than 0.33 are considered selective; their *PD* response was at least twice as great as their *NPD* response. For each cell, we also used a *t*-test (criterion *P*-value <0.05) to compare mean responses to opposite directions of motion, in order to evaluate the significance of the *DI*.

Our analysis of the counterphasing grating data was designed to summarize the S-T orientation of cells' receptive fields, and to estimate the contribution that a strictly linear receptive-field mechanism makes to direction selectivity. For such a mechanism, S-T structure completely determines directional tuning. Our use of counterphasing gratings is similar to previous studies (Albrecht & Geisler, 1991; Reid et al., 1991) but most of our analyses are tied more closely to response phase (i.e. timing). Here we first describe the rationale for the procedure and how it is performed. To compare our results directly with those of other studies, we also employed a more conventional method of linear prediction that used response phase and amplitude; that method is described second.

Predictions based on a strictly linear model

Figs. 1A and 1B illustrate the responses of a hypothetical, strictly linear, fully direction-selective simple cell to a counterphasing grating at 16 positions in the receptive field. First harmonic amplitudes and response phases are plotted as a function of grating position, which is measured in cycles. As the spatial phase of the grating shifts, response amplitude remains constant (*A*) but response phase covaries with spatial phase (*B*), revealing a spatiotemporally oriented receptive field. These responses can be understood by considering the nature of the stimulus. A counterphasing grating consists of two superimposed sine-wave gratings drifting in opposite directions. Shifting the spatial phase of the stationary grating consists of altering the starting position of each drifting component. A fully direction-selective cell responds exclusively to one of the components, producing a constant amplitude regardless of spatial phase. Shifting the spatial phase delays or advances the response to that component by an amount equal to its spatial displacement. Thus, for a completely direction-selective cell the relation between response phase and spatial phase is described by a line with unity slope (Fig. 1B).

Responses of a linear, nondirection-selective cell are shown schematically in Figs. 1C and 1D. As the spatial phase of the

grating shifts, response amplitude varies sinusoidally in each half-cycle. Here each component of the stimulus produces a response, and their interaction generates the sinusoidal variation in amplitude. When the component sine waves are perfectly in phase a maximum response is produced. For the data in Fig. 1C this corresponds to 0.25 cycles; symmetry also produces a peak at 0.75 cycles. A gradual increase or decrease in spatial phase from these optima causes the two stimulus components, and their elicited responses, to gradually move out of phase, yielding smaller net response amplitudes. When the components are completely out of phase, at 0.5 cycles, they elicit responses that completely cancel. In contrast, response phase remains constant except for a half-cycle jump that reflects a half-cycle shift in the stimulus. The slope of a line fit to the phase data in each half-cycle therefore is 0; the receptive field lacks space-time orientation. Constant temporal phase is caused by symmetric displacement of the two stimulus components in opposite directions starting from the optimum spatial phase. This elicits two symmetric responses, a phase lead and lag, which cancel.

For intermediate directional tuning, the profiles of response amplitude and phase resemble a weighted combination of the two extreme cases above. Amplitude fluctuates but remains nonzero; an amplitude ratio, defined as (min amp/max amp), lies between 0 and 1. The temporal phase data do not follow a straight line but are described by an arctangent function:

$$\varphi(\psi) = \varphi_0 + \frac{1}{2\pi} \tan^{-1} \left(\frac{\tan(2\pi(\psi - \psi_0))}{STI} \right) \quad (2)$$

where $\varphi(\psi)$ is the temporal response phase at spatial phase ψ ; φ_0 and ψ_0 are arbitrary constants describing the temporal and spatial offsets, respectively, of the receptive field with respect to the stimulus. The parameter *STI* (i.e. S-T index) describes the degree of S-T orientation in the receptive field; it varies from 0 to 1. We used this function to fit the temporal phase *versus* spatial phase data in each half-cycle, with the three parameters φ_0 , ψ_0 , and *STI*, free to vary. Examples of these fits are illustrated in Fig. 5. A detailed derivation of the fitting function is given in the Appendix.

In a strictly linear model, either the *STI* or the amplitude ratio suffice to predict direction selectivity. However, as noted by others (e.g. Albrecht & Geisler, 1991) static nonlinearities accentuate the amplitude modulation of responses to counterphasing gratings and lead to an underestimation of direction selectivity. Since response phase is not affected by these nonlinearities, we relied primarily on it to summarize the linear component of direction selectivity.

Conventional linear predictions based on amplitude and phase

We also used the superposition method of Jagadeesh et al. (1993) to predict direction selectivity based on both the amplitude and phase of responses to counterphasing gratings at different spatial phases. From the average predicted responses, we computed a predicted directional index as in eqn. (1); index values vary from 0 to 1.

For ease of viewing, we normalized all the counterphase data in two ways: (1) the response amplitude and phase functions were shifted equally horizontally so that amplitude peaked at 0.25 and 0.75 cycles, and (2) the response phase functions were shifted vertically to pass through the origin.

Statistics

Unless stated otherwise, all statistical comparisons were made using the Mann-Whitney *U* test (Siegel, 1956).

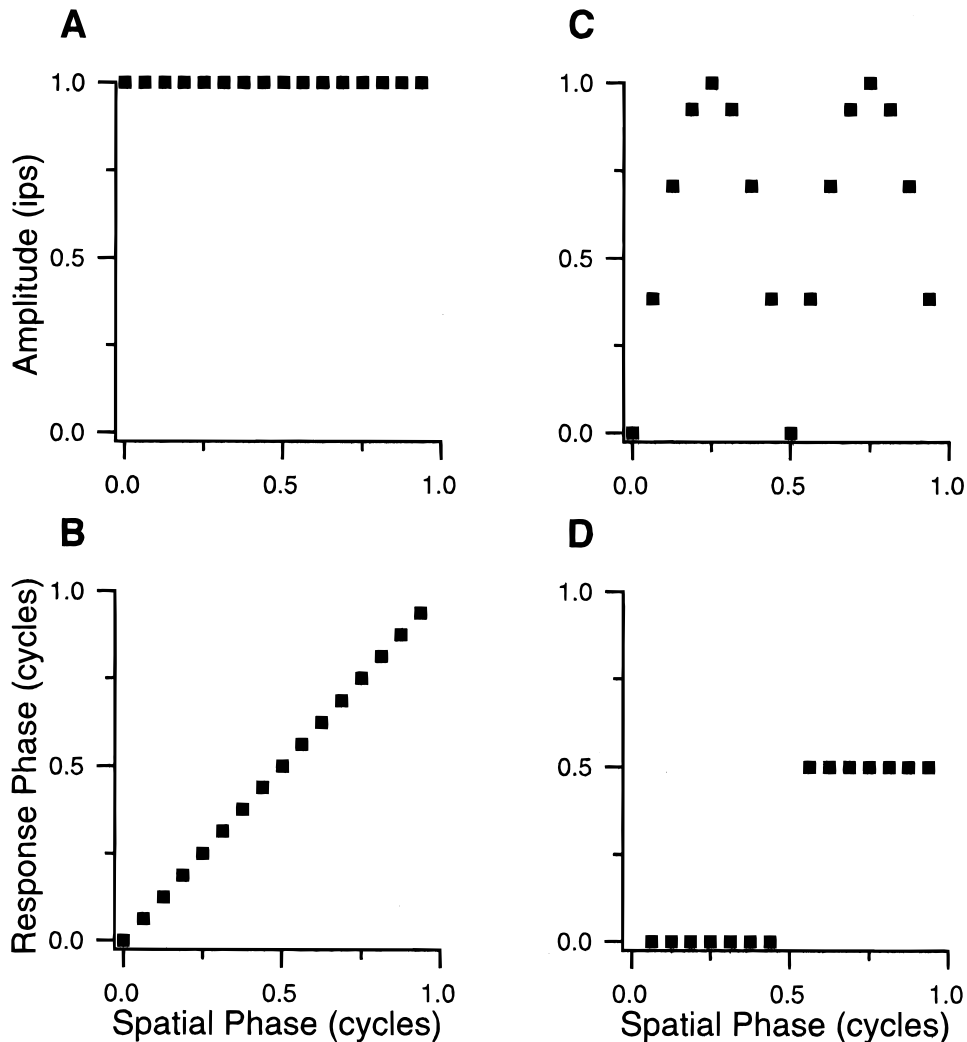


Fig. 1. Theoretical responses of two cortical cells as a function of the spatial phase of a counterphasing grating. Strictly linear summation across the receptive field is assumed. A,B: For a completely direction-selective cell, normalized response amplitudes are constant (A) and response phase increases monotonically with a slope of 1 (B). C,D: For a nondirection-selective cell, amplitudes vary as the absolute value of a sine function with a null at 0 and 0.5 cycles (C), while response phase in each half-cycle is constant except for a half-cycle jump (D) that reflects a half-cycle temporal displacement of the grating.

Reconstructing laminar locations of recorded cells

Electrode penetrations were marked by extracellular deposits of Pontamine sky blue or horseradish peroxidase to aid in reconstructing the tracks. At the end of each experiment the animal was killed using an overdose of Nembutal (Abbott Labs, North Chicago, IL) and perfused with aldehydes (Humphrey et al., 1985). The brain was sectioned, processed for HRP if necessary, and stained for Nissl substance. Electrode tracks were reconstructed at 100 \times using a microscope with a camera lucida.

Laminar borders in area 17 were identified according to the criteria of O'Leary (1941), as summarized by Humphrey et al. (1985), and cells' recording locations assigned accordingly. Layer 4 consists of two divisions. Layer 4A contains loosely packed, small- and medium-sized stellate and pyramidal cells; its border with layer 3 is identified by the presence of large pyramidal cells. Cells recorded in the border zone between layers 3 and 4 did not differ from layer 4A cells and so they are grouped with layer 4A for

analysis. Layer 4B consists primarily of tightly packed, small stellate cells; its boundary with layer 4A is roughly identified by differences in cell size and density in the two divisions and by occasional large round, or oval-shaped cells lying at the base of layer 4A. The border between layers 4B and 5A occurs at the level of the apices of the most superficial large pyramids in layer 5B, which invade layer 5A, a narrow strip of small and medium pyramidal-shaped neurons. Layer 5A is visible near the apex of the lateral gyrus but is difficult to distinguish from layer 4B along much of the medial bank of the gyrus. Because of this uncertainty, the few ($n = 3$) cells localized to layer 5A and the 4/5 border were grouped with layer 4B. Layer 6 consists of densely staining medium pyramids and fusiform cells grouped into radial clusters. The clustering drops off rapidly at the border with layer 5.

Most cells were recorded along the medial bank of the lateral gyrus where the electrodes passed through cortical layers at oblique angles. This greatly reduced potential errors in assigning recording sites because the electrodes remained within individual

layers for extended distances, up to 3 mm in many cases. We are highly confident of most cell placements. Cells whose placements were problematic are excluded from the laminar analyses but are included in other summaries.

Results

We recorded from 101 simple cells in area 17. Laminar classification yielded 26 cells in layer 4A, 27 cells in layer 4B, and 22 cells in layer 6. A few cells were recorded in midlayer 3 ($n = 11$) and in 5B ($n = 4$) but they are excluded from the laminar analyses, as are 11 cells with unknown locations. These 26 cells are included in the population summaries.

We will first describe the S-T structure of direction-selective cells and our measure of S-T orientation. We will then document the laminar variations in S-T orientation and their relation to direction selectivity. Then we will evaluate the adequacy of an LN model for different cortical layers.

S-T structure of direction-selective simple cells

The responses of a direction-selective cell in layer 4 to a stationary counterphasing grating at various spatial phases across the receptive field are shown in Fig. 2A. The sinusoidal luminance profiles illustrated below the responses indicate a temporal frequency of 4 Hz, which was optimal for the cell. For clarity, two cycles of stimulation are shown. The grating elicited a robust, well-modulated discharge at all positions.

Together these responses describe the S-T structure of the receptive field, which was characterized by a gradual change in response timing as a function of stimulus spatial phase. The response phase progressively increased over the first half-cycle and the pattern was repeated over the second half. This is an example of an S-T oriented receptive field. This type of organization was first described by Movshon et al. (1978) who interpreted the response pattern as reflecting a linear receptive field possessing different response timings. That interpretation has been substantiated

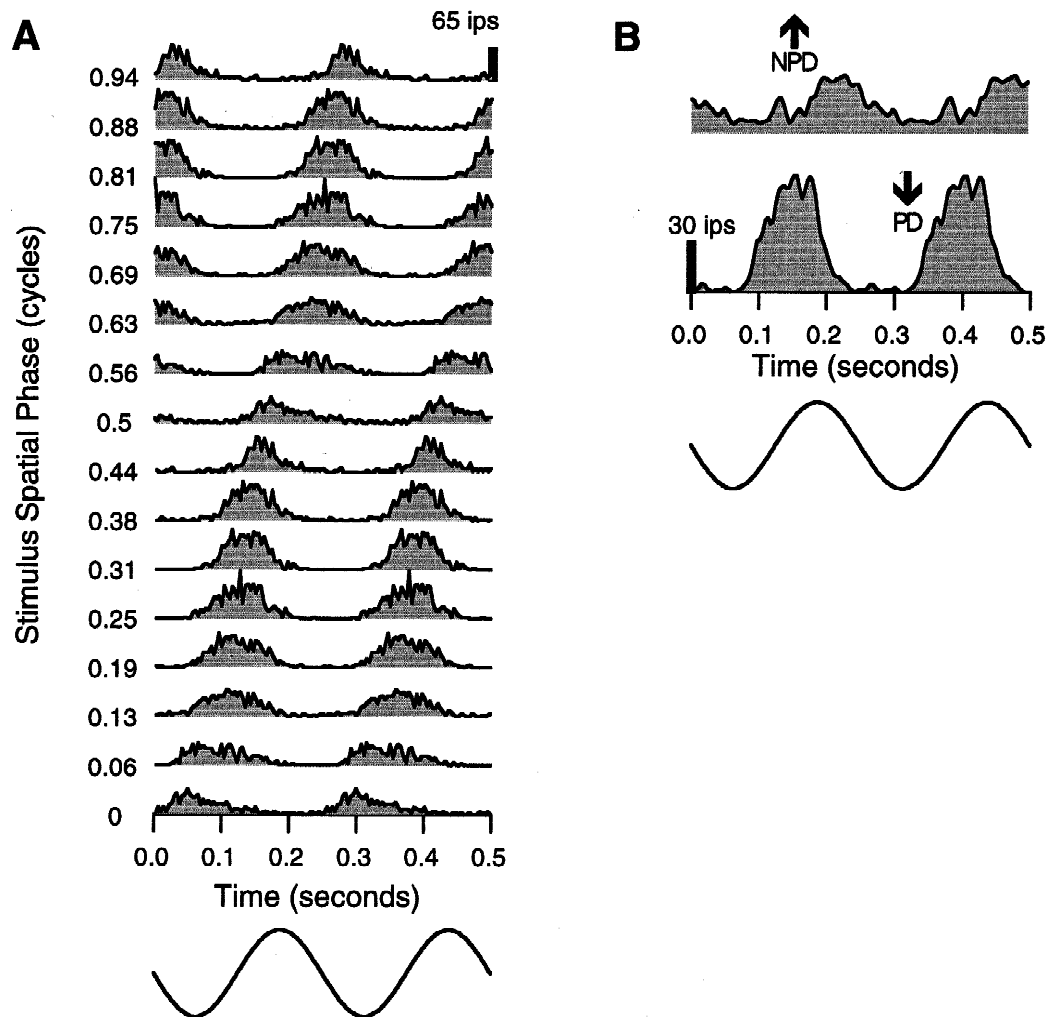


Fig. 2. Average responses of an S-T oriented, direction-selective cell in layer 4B to sine-wave luminance-modulated gratings presented at 4 Hz. The luminance profile over time is illustrated below each set of PSTHs. Two cycles of stimulation are shown for clarity; the second response in each PSTH is a duplicate of the first. Calibration bars indicate firing rates in impulses/s. A: Responses to a counterphasing grating at 16 spatial phases spanning a full cycle. The first half-cycle was tested; symmetry allowed the responses to be duplicated to complete the second half-cycle. Note that as spatial phase increased, responses were gradually delayed. B: Responses to a grating drifting in opposite directions; the *DI* was 0.65.

by others using a variety of receptive-field mapping methods (McLean & Palmer, 1989; Reid et al., 1991; Saul & Humphrey, 1992a).

The cell's response to a grating drifting in opposite directions is illustrated in Fig. 2B. It was moderately direction selective, having a *DI* of 0.65. As noted in other studies (McLean & Palmer, 1989; Reid et al., 1991), the preferred direction can be ascertained from the static receptive-field maps. Coincident temporal integration of excitatory responses occurred optimally only for a stimulus moving from top to bottom through the receptive field, successively activating regions with progressively shorter latencies, or earlier response phases. This produced a larger response than movement in the opposite direction, where less excitatory temporal integration occurred. Thus the cell's direction selectivity can be attributed qualitatively to S-T orientation. A similar relation holds for most direction-selective cells in layer 4.

Another example of a direction-selective cell, located in layer 6, is illustrated in Fig. 3. Although completely selective, its receptive field displayed very little S-T orientation; timing was nearly uniform across the receptive field except for a half-cycle jump at about spatial phase 0.5. The cell's strong direction selectivity can-

not be attributed to first-order receptive-field structure since it is quite S-T unoriented.

Quantitative evaluation of S-T orientation

Simple-cell receptive fields varied widely in their S-T structure, in agreement with previous reports (Reid et al., 1991; Albrecht & Geisler, 1991). To quantify each cell's behavior in this regard, we Fourier analyzed its responses to counterphasing gratings and plotted the first harmonic response phases and amplitudes against stimulus spatial phase. The plots in Figs. 4A and 4B are derived from the layer 4 cell in Fig. 2A. Response phase varied monotonically with spatial phase, as would be expected for an S-T oriented receptive field. To quantify this orientation, we fit the response phase *versus* spatial phase data with the arctangent function in eqn. (2). The fit, shown as a solid line in Fig. 4A, yielded an *STI* of 0.46. The mean response amplitudes (Fig. 4B) showed some modulation as a function of grating position but there was no null phase (i.e. no spatial phase eliciting zero response).

Figs. 4C and 4D show similar plots for the layer 6 cell in Fig. 3. Response phase changed only slightly across spatial phase except

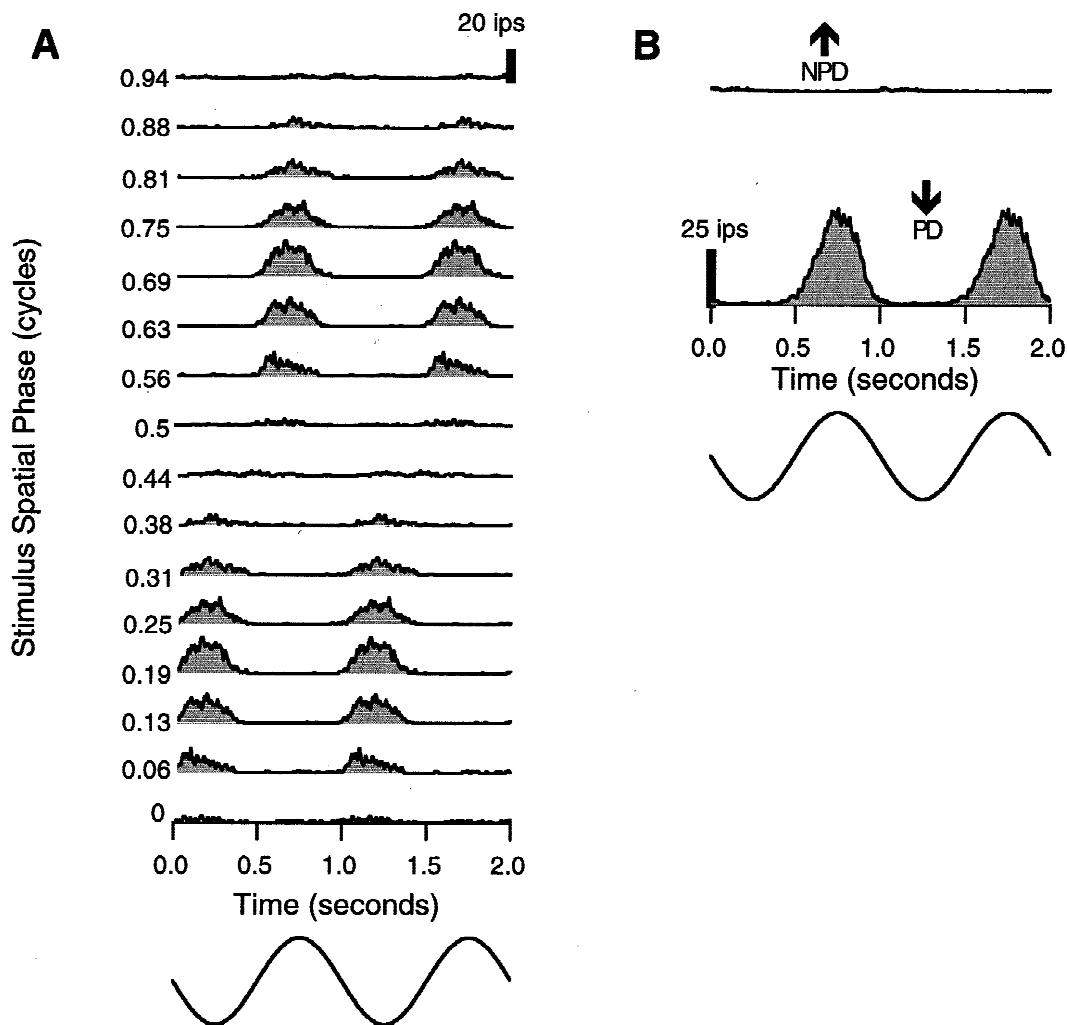


Fig. 3. Responses of a direction-selective cell in layer 6. The format is the same as in Fig. 2 but with 1-Hz luminance modulations. A: Unlike the previous example, response timings across the receptive field were very similar except for a half-cycle jump. B: Despite being S-T unoriented, the cell was direction selective (*DI* = 0.95) to drifting gratings.

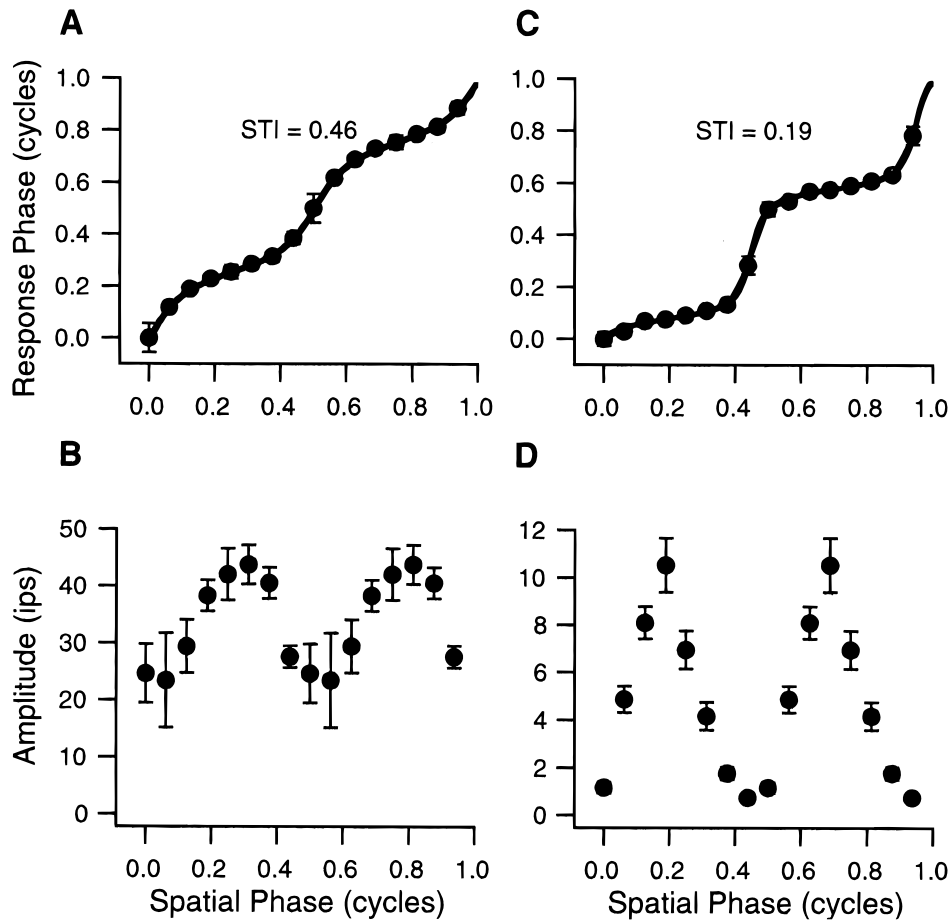


Fig. 4. A,B: Responses of the layer 4 cell in Fig. 2 to counterphasing gratings. Average response (\pm S.E.M.) temporal phase (A) and amplitude (B) are plotted as a function of stimulus spatial phase. The responses are typical of an S-T oriented receptive field: as stimulus spatial phase increased there was a monotonic increase in response phase and some modulation in amplitude that did not include a null response. An arctangent fit to the phase data (solid line in A) yielded an *STI* of 0.46, which is the linear prediction of direction selectivity. C,D: Responses of the layer 6 cell in Fig. 3. Amplitude fluctuated as a fully rectified sinusoid with a near null phase (D), and a prominent S-T gradient was absent (C). The fit to the phase data yielded an *STI* of 0.19. The response profiles were typical of a nondirection-selective cell but the neuron was highly selective (*DI* = 0.95).

for the roughly half-cycle shift midway through the spatial progression. The arctangent fit yielded an *STI* of 0.19. The amplitude profile was sinusoidal within each half-cycle, with a near null response at 0.5 cycles. Both the phase and amplitude profiles are characteristic of a linear nondirection-selective cell. The cell's strong direction selectivity (*DI* = 0.95) could not be attributed to linear S-T mechanisms because they would predict a *DI* of only 0.19.

Typical examples of response-phase *versus* stimulus-phase relationships for 12 additional cells are illustrated in Fig. 5. Also shown for each cell is the arctangent fit (solid line), *STI* and *DI*. Each column in the figure is organized from left to right such that cells belong to layers 4A, 4B, and 6, respectively, and from bottom to top such that direction selectivity increases. For cells in all layers the fits were quite good. For nondirection-selective cells there were no differences among laminae; nearly all cells had *STIs* less than 0.2. Differences were seen only when direction-selective cells were considered: phase profiles in layer 4 displayed prominent S-T orientation whereas those in layer 6 did not.

Laminar differences in S-T orientation

We next examined *STI* as a function of cortical layer for the whole population, excluding cells that were not direction selective. As

shown in Figs. 6A and 6B, cells in layer 4 displayed a wide range of *STIs*, from 0 to 0.8. The mean *STI* (0.43) for layer 4B, however, was greater than that for layer 4A (0.26). The difference between the distributions was significant ($P < 0.05$). Layer 6 was strikingly different in that all direction-selective cells had low *STIs* (Fig. 6C), which ranged from 0 to 0.3. The mean *STI* (0.13) was lower than that of either subdivision of layer 4, and the *STI* distribution was significantly different than that in layer 4A or 4B ($P < 0.05$). The greatest difference occurred between layers 4B and 6, where the overlap in *STI* values was very low.

These laminar variations in S-T orientation did not reflect differences in direction selectivity. Figs. 6D–6F show the distributions of *DI*s across layers. About 80% of cells in each layer were direction selective and their mean *DI*s (~ 0.74) were nearly identical. These results thus suggest a laminar basis for the well-known variable relationship between direction selectivity and receptive-field structure. We examine this relationship next.

Laminar differences in the correlation between S-T structure and direction selectivity

The scatter plots in Fig. 7 show how *STI* and direction selectivity relate as a function of layer. Each point represents a single cell. In

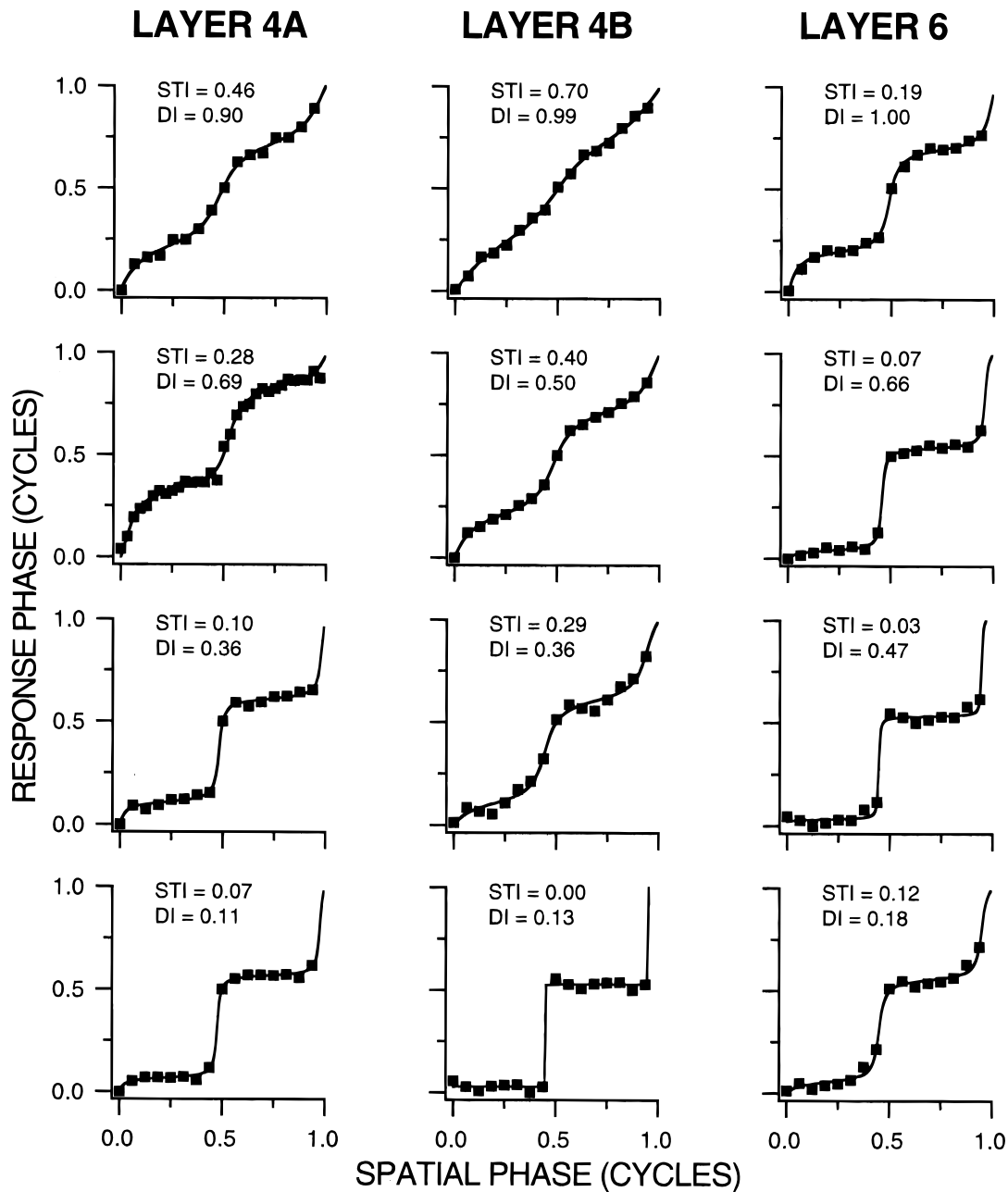


Fig. 5. Plots of response phase as a function of the spatial phase of a counterphasing grating, for 12 typical cells. Curves through each set of data are the arctangent fits generated by the linear S-T model. The resulting values of S-T orientation are shown along with the measured direction selectivities (DI). Cells are grouped into columns according to layer, with DI increasing from bottom to top in each column. There was no laminar difference in S-T orientation among cells with low DI s; all were S-T unoriented. At higher DI s, S-T orientation generally increased in layer 4 but remained low in layer 6.

layer 4B (Fig. 7B), the correlation between the two measures was high ($r = 0.76$) and the slope of a regression line was 0.5. The dashed line of slope 1 indicates a perfect correlation, keeping in mind that in a strictly linear model the degree of S-T orientation completely determines direction selectivity. Thus, linear mechanisms account for about half of the observed directional tuning in layer 4B. On closer inspection one notices that the greatest discrepancies between STI and measured direction selectivity occurred for cells with high DI s (>0.7). For DI s less than 0.7, STI provided a much better prediction, and a linear mechanism could account for 74% of the directional tuning.

In layer 4A (Fig. 7A), the relation between STI and direction selectivity was more variable ($r = 0.48$) and the slope of the best fit line was 0.24. In layer 6 another picture emerged (Fig. 7C). There was no correlation between the two measures ($r = 0.16$) and the slope was quite low (0.06). Nearly all cells had low STI values no matter what their directional tuning. This implies that gradients in response timing are too weak to account adequately for direction selectivity in layer 6.

Fig. 7D plots STI versus DI for the entire sample. The result of combining laminae results in an overall low correlation ($r = 0.48$) due to heterogeneity, and a slope of 0.31. The population

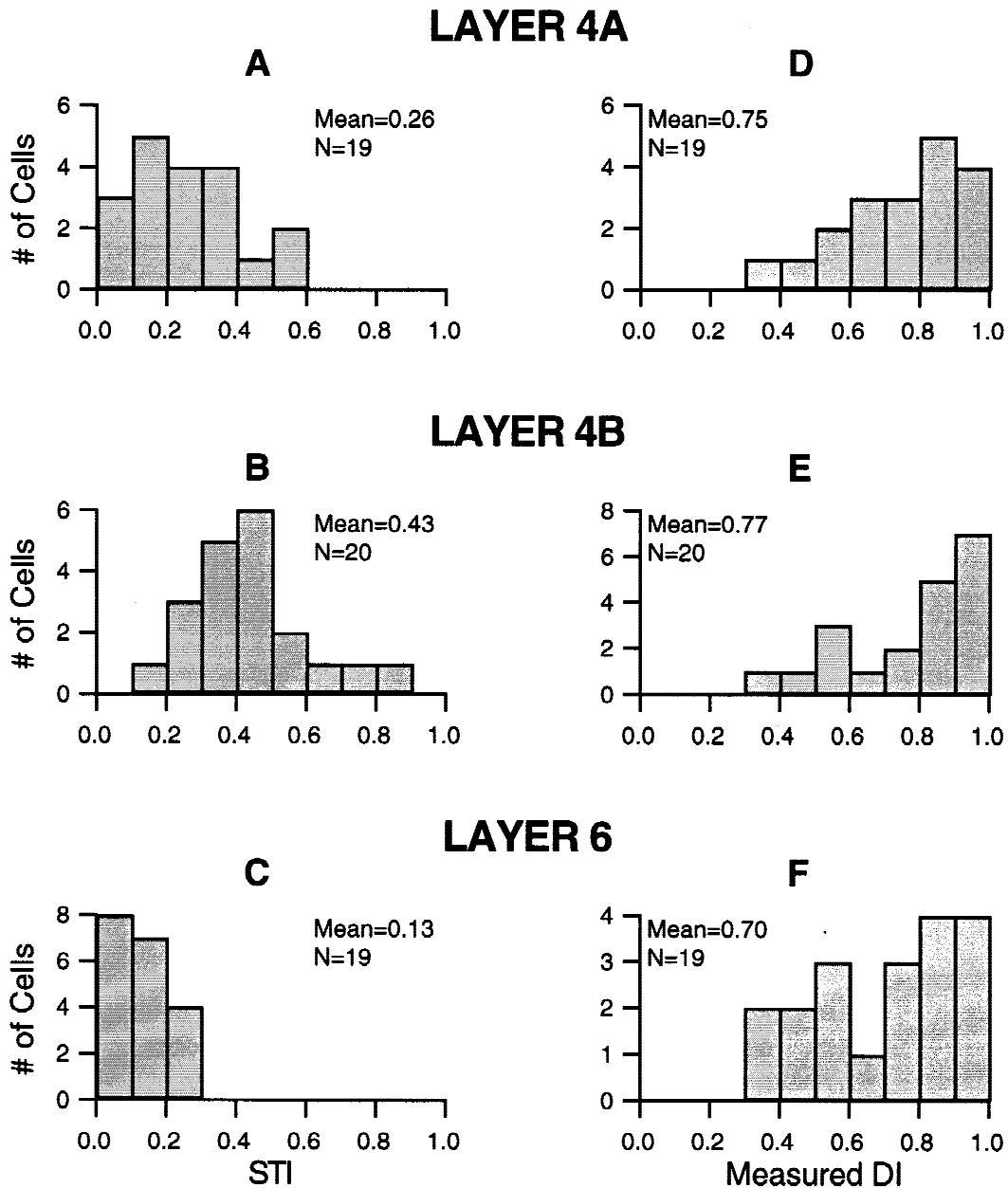


Fig. 6. A–C: Frequency distributions of *STI* values for direction-selective cells in each layer. Means and sample sizes are indicated. On average, the highest and lowest S-T orientations were observed in layers 4B and 6, respectively. Layer 4A was intermediate. D–F: Corresponding laminar distributions of *DIs* measured with drifting gratings for cells that were direction selective. The distributions were nearly identical across layers and thus cannot account for the differences in S-T orientation.

heterogeneity thus can be attributed partly to cells' laminar locations.

In addition to quantifying S-T orientation from plots of response phase, we used the superposition principle to compute a predicted *DI* based on response phase and amplitude. Fig. 8 shows scatter plots of predicted *versus* measured *DI* for each layer. As in Fig. 7, laminar differences existed, especially between layers 4B and 6. A significant correlation ($P < 0.05$ on Spearman rank correlation test) was observed in layer 4 ($r = 0.59$ in 4B; $r = 0.51$ in 4A) but there was no correlation in layer 6 ($r = -0.01$). Combining all data (Fig. 8D) yielded a low correlation ($r = 0.40$) and the slope of the regression line was 0.23. Roughly similar population values have been reported by others for simple cells in cat

area 17 (Albrecht & Geisler, 1991; Reid et al., 1991; DeAngelis et al., 1993b; McLean et al., 1994). Finally, we note that the *STI* values in layer 4 tended to be slightly higher than the values for conventional linear predictions. This is expected because the latter measure reflects the distorting effects of static nonlinearities on response amplitude.

Accuracy in predicting preferred direction of motion

Although the above data reveal differences among laminae, all but three cells in Figs. 7D and 8D lay in the first quadrant, where the signs of the predicted and measured *DIs* matched. Thus regardless of laminar location, S-T orientation almost always correctly pre-

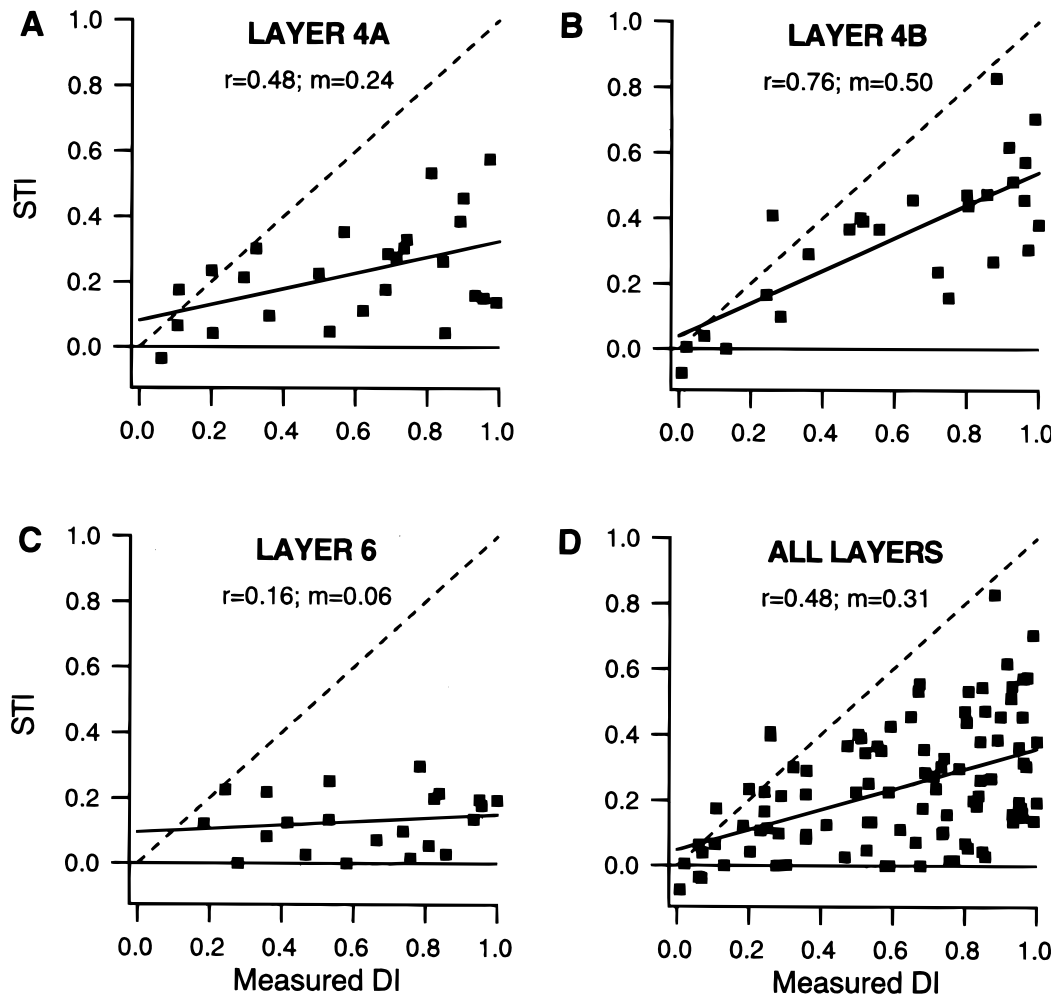


Fig. 7. Laminar differences in the relation between direction selectivity and S-T orientation. Each point in the scatter plots represents a cell. All cells, direction-selective or not, are included. The dashed lines of unity slope indicate the ideal relationship assuming a strictly linear S-T model. Negative values of *STI* reflect incorrect estimates of the preferred direction of stimulus motion. The solid lines are best fits to the data, from which the slopes (*m*) and correlation coefficients (*r*) were derived. A–C: The correlations were highest in layer 4B, least in layer 6, and intermediate in layer 4A. D: Pooling data across laminae yielded a moderately low correlation. Thus, some of the heterogeneity between the two measures across the population is attributable to cells' laminar locations. Numbers of cells in A–D are 26, 27, 22, and 101, respectively; *y* intercepts are 0.08, 0.04, 0.10, and 0.05, respectively.

dicted the preferred direction of motion. The three cells with incorrect predictions were not reliably tuned for direction. In general, *DIs* < 0.1 did not differ from zero ($P < 0.05$ on *t*-test), whereas *DIs* > 0.1 did.

Evaluation of an LN model of direction selectivity

These data confirm that linear predictions of direction selectivity are correlated with measured values in layer 4, although discrepancies exist for nearly all cells, particularly in layer 6. Such discrepancies often have been attributed to static nonlinearities, which are modeled as thresholds and/or expansive nonlinearities (McLean & Palmer, 1989; Albrecht & Geisler, 1991; Reid et al., 1991; Tolhurst & Dean, 1991; DeAngelis et al., 1993b; Heeger, 1993). We examine here the ability of one class of LN models ("exponent model"; Albrecht & Geisler, 1991; Heeger, 1993) to account for direction selectivity in our cells. The model consists of a linear filter followed by a power-law amplification of suprathreshold

responses. The only parameter is the exponent, which is typically on the order of 2 ("half-squaring," Heeger, 1993). To test the model, we compare two independently derived exponents. One is the exponent required to match direction selectivity linearly predicted from counterphasing gratings to that measured with drifting gratings; we refer to this exponent as n_{DG} . The other exponent, n_{CG} , is determined by predicting the modulation of response amplitude to counterphasing gratings that is attributable to a linear mechanism, and comparing this to the measured modulation. If an exponent model is correct, then these two exponents should be equivalent. We will show that the exponent model could work for most cells in layer 4, but that it fails in layer 6 because receptive fields there are only weakly oriented in space-time.

To obtain n_{DG} we calculated the exponent required to bring the predicted and measured *DI* for each cell in Fig. 8 into correspondence; i.e. to move the points to the diagonal. The calculations were nearly identical to those used by DeAngelis et al. (1993b). Fig. 9 shows the distribution of these exponents in each layer and

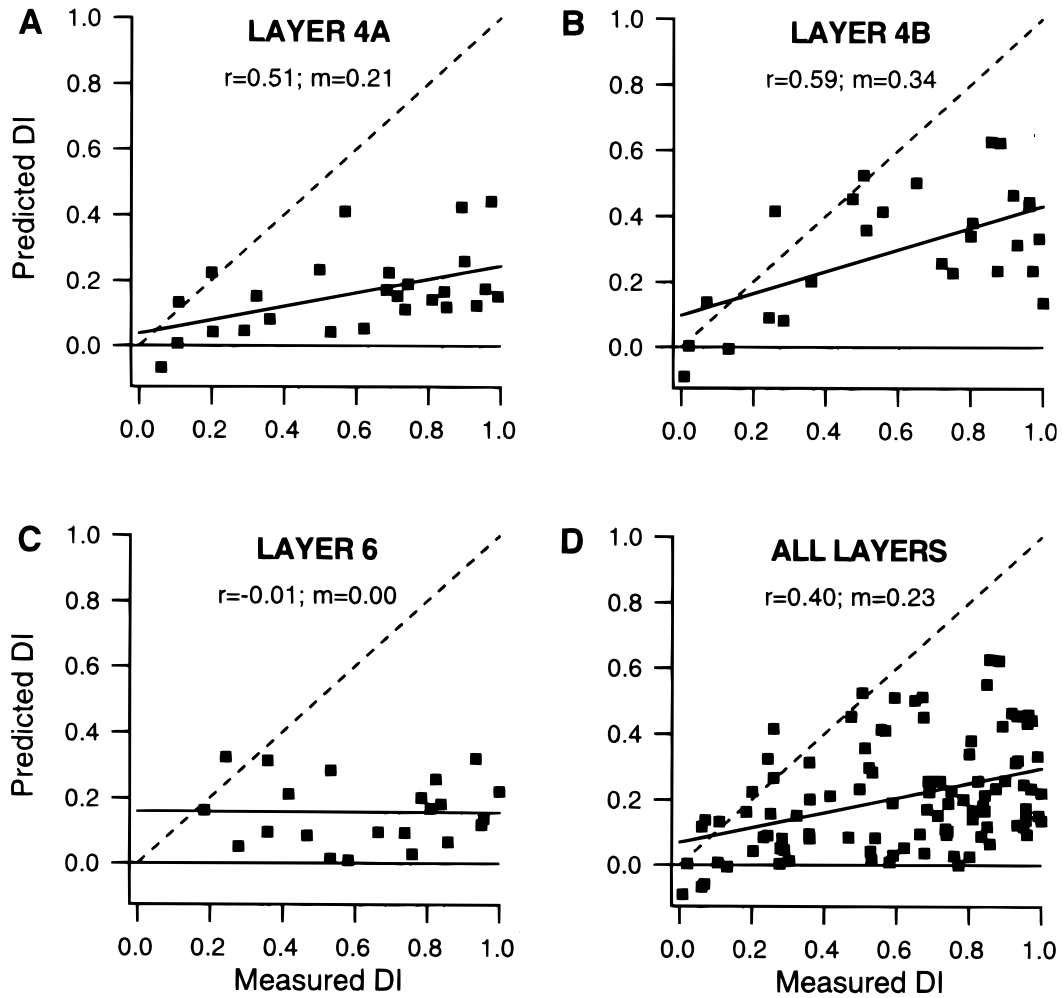


Fig. 8. Laminar differences in the relation between direction selectivity and conventional linear predictions based on response amplitude and phase to counterphasing gratings. The format is similar to Fig. 7. A–C: As with the *STI* measure, the correlations with direction selectivity were highest in layer 4B, lowest in layer 6, and intermediate in layer 4A. D: When combining cells in all laminae the correlations were weaker. The y intercepts in A–D are 0.04, 0.10, 0.16, and 0.07, respectively.

for the whole population of direction-selective cells. This population distribution is similar to those reported previously (Albrecht & Hamilton, 1982; DeAngelis et al., 1993b). The large values (>4) correspond to direction-selective cells with little S-T orientation. Such cells require a strong nonlinear contribution to make up for the weak linear directional component. Exponents near 1 indicate cells for which the linear prediction was close to the actual *DI*; these cells lie near the diagonal in Fig. 8. There was considerable overlap in exponent values across layers, but on average n_{DG} was lowest in layer 4B (geometric mean = 2.2), highest in layer 6 (4.0) and intermediate in layer 4A (3.3), as expected based on Fig. 8. From these data alone, an exponent model could in principle account for direction selectivity in all layers, although large exponents (e.g. >4) would be required for many cells in layer 6 and a few cells in layer 4. However, further insight is gained by additional analysis.

If the model being considered has predictive power, then the exponent for each cell in Fig. 9 should be similar to the exponent, n_{CG} , derived from counterphasing grating responses. We computed n_{CG} for each cell by comparing the *STI* value, calculated solely from response phase data, to the degree of measured amplitude

modulation. An amplitude ratio was defined as A_{\min}/A_{\max} ; the values corresponded to the minimum and maximum amplitudes evoked by stationary gratings. Because the static nonlinearity parametrized by the exponent does not affect phase by definition, the *STI* was already linearized. Thus, we simply found the exponent, n_{CG} , that when applied to the *STI* matched the amplitude ratio. As described in the Appendix, this consisted of fitting

$$A(\psi) = A_{\max} \{ \sin^2[2\pi(\psi - \psi_0)] + STI^2 \cos^2[2\pi(\psi - \psi_0)] \}^{n/2} \quad (3)$$

to the measured amplitude *versus* spatial phase data. Here, ψ_0 is the null spatial phase, and n is the parameter whose value is optimized to obtain n_{CG} . Unique values of n_{CG} were obtained for all cells.

Figs. 10A and 10B illustrate this procedure as it was applied to a direction-selective cell in layer 4. The *STI* was 0.51, which *via* eqn. (3) with $n = 1$ generated the dashed curve in B, representing the linearized amplitude (i.e. amplitude ratio = 0.51). To fit the actual modulated response shown as solid squares in B, these amplitudes, normalized by dividing by A_{\max} , had to be raised to a

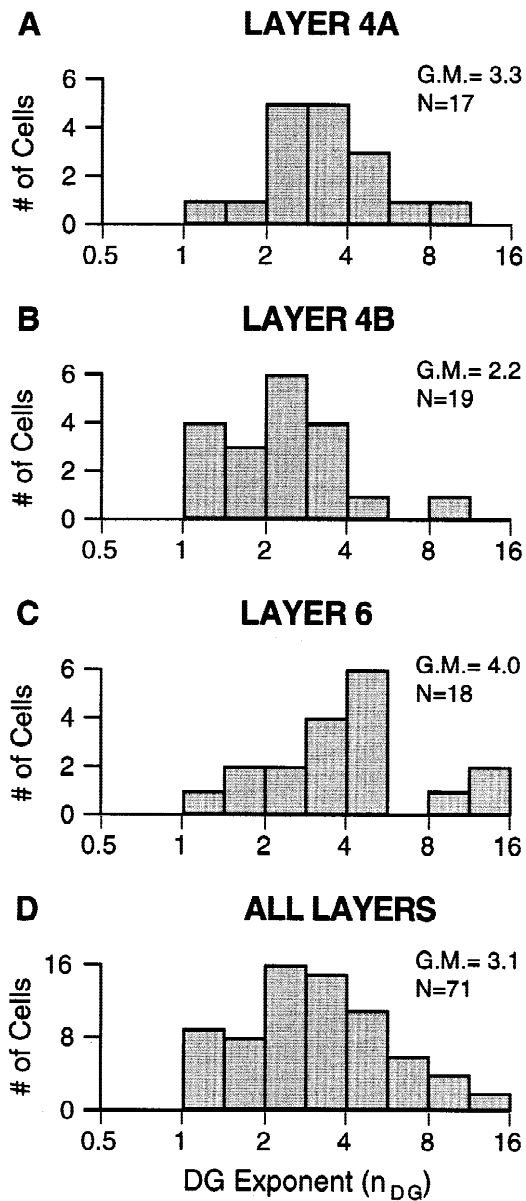


Fig. 9. Frequency distributions of the exponents, n_{DG} , required to bring the predicted and measured DIs in Fig. 8 into perfect correspondence. Only direction-selective cells are shown. A–C: On average n_{DG} was lowest in layer 4B and highest in layer 6. The distributions in these two layers were significantly different ($P < 0.05$). Values of n_{DG} in layer 4A were intermediate; they differed significantly from those in layer 4B ($P < 0.05$) but not from those in layer 6. D: The distribution for all layers was very similar to that of Albrecht and Hamilton (Fig. 13, 1982) and DeAngelis et al. (Fig. 11C, 1993b).

power of 3.0. This generated the solid curve that has an amplitude ratio of 0.13 (i.e. $0.51^{3.0}$).

The direction-selective cell in layer 6 shown in Figs. 10C and 10D was fit best by an exponent of 1.4. The value is close to 1 because of the relatively small discrepancy between the STI (0.1) and the amplitude ratio, which was 0.04 (i.e. $0.1^{1.4}$). This is typical of layer 6 cells, where the low STI values were consistent with the low amplitude ratios, even though neither set of values was consistent with measured direction selectivity in most cases.

The distribution of n_{CG} for each layer is shown in Figs. 11A–11C. As a population, these exponents tended to be lower than n_{DG} (Fig. 9), especially in layer 6. This is contrary to the exponent model, under whose assumptions these independent estimates should be equivalent. We compared the two estimates for individual cells by taking their ratio (n_{DG}/n_{CG}), as shown in Figs. 11D–11F. Although there is overlap among the layers, this ratio was centered approximately near 1 for layer 4 but was shifted well to the right for layer 6, indicating large discrepancies between the two exponents. On average, the ratios were significantly higher in layer 6 than in either division of layer 4 ($P < 0.05$).

Finally, we examined the effect that large exponents would have on responses to counterphasing gratings. The value of n_{DG} for the layer 6 cell in Fig. 10D was 4.8, much higher than n_{CG} for the cell. The dotted curve in D plots eqn. (3) using this larger exponent. Although the amplitude at the null phase was affected little by the higher exponent, because it was already small, amplitudes between the optimal and null phases were decreased. Thus, large exponents would tend to produce weak or no responses to counterphasing gratings except near the optimal spatial phase. However, this was not observed experimentally; most cells responded well over a large range of spatial phases (e.g. Fig. 3A). The layer 4 cell in Fig. 10B gave similar values of n_{CG} and n_{DG} , and therefore the solid and dotted curves overlap substantially.

The exponent model therefore is consistent with the data from most cells in layer 4, but fails in layer 6. Direction-selective cells in layer 6 are not spatiotemporally oriented, and so would require large exponents to amplify the small difference between the directions created by the linear response component. However, these large exponents would be expected to affect the amplitude modulation in response to counterphasing gratings in a manner that is not observed. Direction-selective simple cells in layer 6, and some in layer 4, must be subject to nonlinearities other than, or in addition to, this power-law nonlinearity. We speculate on what these might be in the Discussion.

Discussion

Our data reveal a laminar basis for the heterogeneity in S-T orientation and its relation to direction selectivity. In this section, we compare our methods and results to those of previous studies, consider our interpretations in light of possible mechanisms, and suggest potential sources for the laminar differences.

Methodology and relation to previous studies

Reid et al. (1987, 1991) were the first to examine systematically the relation between S-T structure and direction selectivity in simple cells. They found a significant correlation ($r = 0.61$) between actual direction selectivity and that based on linear predictions from responses to counterphasing gratings. Similar correlations were obtained by Albrecht and Geisler ($r = 0.70$; 1991), and by McLean et al. ($r = 0.45$; 1994) and DeAngelis et al. ($r = 0.46$; 1993b) using briefly flashed bars. The population correlations we observed were 0.48 for STI versus DI , and 0.40 for linear predictions versus DI . In contrast, Tolhurst and Dean (1987), using counterphasing gratings, found no correlation ($r = 0.19$) between predicted and measured direction selectivity. Thus, a wide range of correlations has been observed.

Our result suggests that laminar differences in receptive-field structure may be a major source of the differences among these studies. Most receptive fields of direction-selective cells in layer

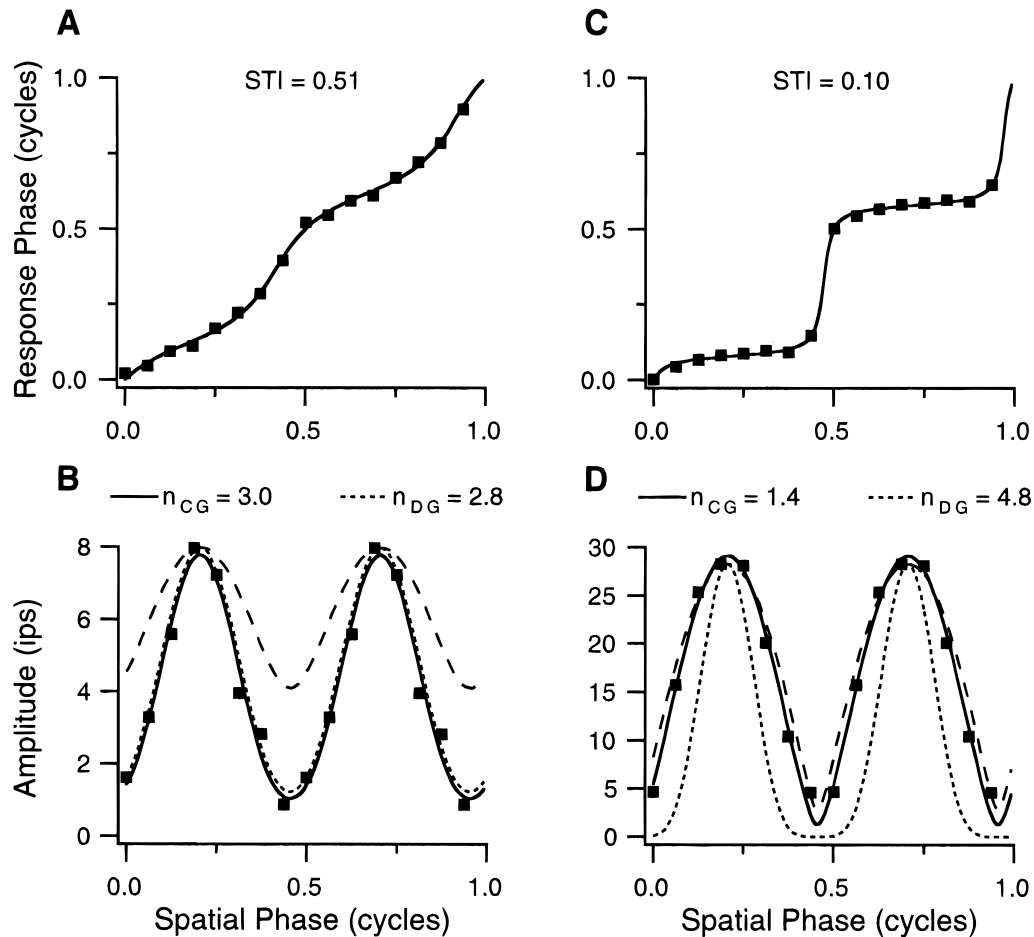


Fig. 10. Estimating the exponent, n_{CG} , of a static nonlinearity from responses to counterphasing gratings. Measured response phase and amplitude profiles (squares) are illustrated for two direction-selective cells. A: The fit to the response phase data from a layer 4 cell yields an STI of 0.51. B: The dashed curve is the expected amplitude profile for the cell based on its STI value. The difference between the measured and linearly estimated profiles is accounted for by an n_{CG} exponent of 3.0. The fit (solid line) to the actual data incorporates the exponent. The dotted line shows predicted amplitude modulation using $n_{DG} = 2.8$. C, D: The same procedure was applied to a layer 6 cell. Here the difference between the expected and observed modulation was much less and a smaller value (1.4) of n_{CG} was required to match the data. The dotted line indicates $n_{DG} = 4.8$.

4B display prominent S-T orientation that correlates moderately well with direction selectivity (Fig. 7B). The correlation is also high when comparing linearly predicted *versus* measured direction selectivity. Cells in layer 6 are at most weakly S-T oriented and there is no correlation with direction selectivity (Fig. 7C). Layer 4A is intermediate with about half the cells displaying clear orientation and the other half weak orientation (Fig. 7A). Some of the discrepancies among earlier studies may be accounted for by laminar sampling biases. The uniformly low predicted directional indices in Fig. 2A of Tolhurst and Dean (1991) could be explained by a recording bias for layer 6 cells. Conversely, the higher correlations between S-T structure and direction selectivity observed by Albrecht and Geisler (1991) and DeAngelis et al. (1993b) could reflect a bias toward layer 4 cells. Indeed, when we reanalyzed our data using the slope measure of Albrecht and Geisler (1991), the new correlation ($r = 0.64$) between slope and direction selectivity for all layer 4 cells was close to that of their population ($r = 0.70$).

Additional differences exist among studies in how well receptive-field structure predicts direction selectivity. For example, the slope of a line relating predicted and measured direction selectivity was lower in Reid et al. ($m = \sim 0.3$; 1991) than in Albrecht and Geisler

($m = 0.52$; 1991), DeAngelis et al. ($m = 0.47$; 1993b), and McLean et al. ($m = 0.56$; 1994). In our study, the population values were 0.31 for STI *versus* DI and 0.23 for linear predictions *versus* DI . Again, some of the variations among studies may be attributed to differences in laminar sampling, but they also reflect methodological differences. Among studies employing counterphasing gratings, Reid et al. (1991) used ratios of response amplitudes at the optimal and orthogonal temporal phases to predict direction selectivity, whereas Albrecht and Geisler (1991) used the slope of a line fit to the response phase *versus* spatial phase data. As shown in Fig. 10, the former method should underestimate directional tuning since it reflects static nonlinearities that exaggerate differences in response amplitude. The slope measure should not be subject to these nonlinearities and hence should more accurately reflect directional tuning. This conclusion is supported by our data in Figs. 7 and 8 for layer 4 cells. The STI (Figs. 7A and 7B) predicts directional tuning somewhat better than the traditional linear predictions (Figs. 8A and 8B). Finally, although the predictions in DeAngelis et al. (1993a,b) and McLean et al. (1994) were based on response amplitudes, their white-noise stimuli probably reduced the influence of nonlinearities.

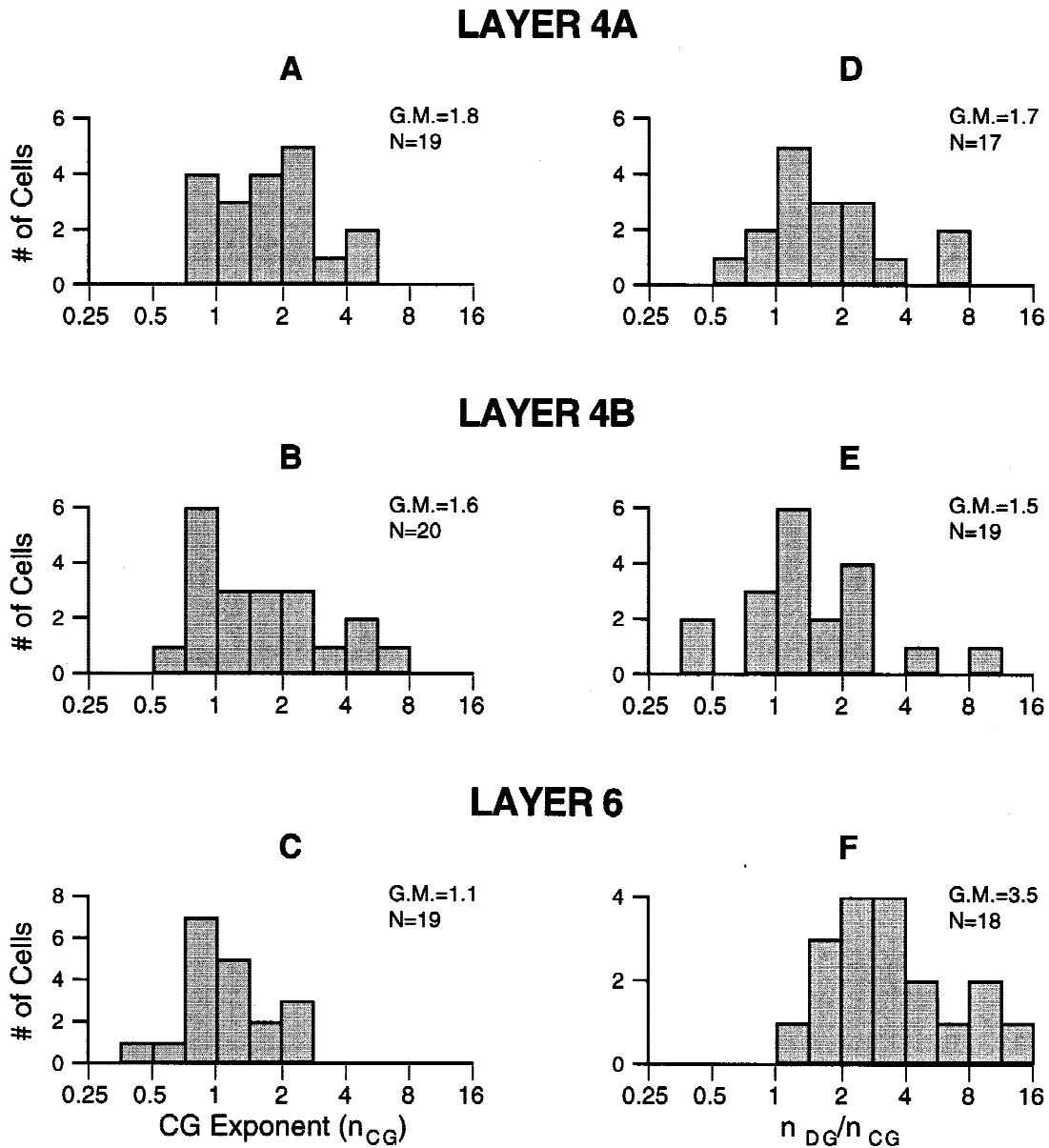


Fig. 11. A-C: Laminar distributions of n_{CG} exponent values for direction-selective cells. D-F: Distributions for the ratio n_{DG}/n_{CG} . On average the discrepancies between the ratios were larger in layer 6 than in layer 4. Differences in cell numbers between A-C and D-F are due to an inability to estimate n_{DG} for four cells.

Evaluation of an exponent model

We evaluated the ability of an LN model to account for differences between linearly predicted and measured direction selectivity. Non-linearities were modeled as exponents, as done by Albrecht and Geisler (1991), although our methods were different. They derived exponents separately from fits to contrast response functions. We estimated them by comparing discrepancies between predicted and measured amplitude modulations in response to counterphasing gratings at a fixed contrast. The amplitude prediction was made possible by the identity of S-T orientation and amplitude modulation in a strictly linear system.

To judge the adequacy of the measured static nonlinearity to account for directional tuning, we compared this exponent, n_{CG} , to another exponent, n_{DG} , that required to match predicted and mea-

sured DIs in Fig. 8. The assumptions are that responses to drifting gratings reflect linear and nonlinear mechanisms, and the exponents derived from Fig. 8 account for all nonlinear processes. For each cell the discrepancy between the two exponents reflects nonlinearities not accounted for by an exponent model. However, the discrepancies provide no direct insight into the types of nonlinearities or their degree of contribution. A fair match existed between n_{CG} and n_{DG} for most cells in layer 4 (Figs. 11D and 11E). Thus, an LN model might account for directional tuning in this layer. In contrast, n_{CG} for layer 6 cells was almost always much smaller than required to match direction selectivity, which implies a failure of this LN model.

Although an LN model was most successful in layer 4B, even there mismatches between predicted and measured exponents occurred. A response threshold (Movshon et al., 1978; Tolhurst &

Dean, 1987) is a potentially powerful enhancement to the model, particularly for cells with DI s approaching 1. Here a threshold almost certainly is required to produce complete response suppression in the nonpreferred direction of motion (e.g. Fig. 3B). While it would be ideal to incorporate both threshold and exponent into the model, the lack of constraints in our data does not permit it; multiple solutions exist.

Nevertheless, might the addition of a static threshold account for direction selectivity in cells with very little S-T orientation, like those in layer 6? It is unlikely. Since only weak selectivity would be established by a linear mechanism, the threshold would have to be not only high but finely tuned to distinguish between responses to opposite directions of motion. For example, Fig. 12A plots a hypothetical membrane potential profile (solid squares) for a cell with an STI of 0.2. It is qualitatively similar to profiles actually recorded (Jagadeesh et al., 1993). Fig. 12B illustrates the resulting linear intracellular response to drifting gratings. To generate complete direction selectivity would require the threshold level (horizontal line in B) to be set between the preferred and nonpreferred intracellular responses, causing complete suppression of action potentials in the nonpreferred direction. Such a threshold should also be invoked in the presence of counterphasing gratings, as indicated by the horizontal line in A. All responses in Fig. 12A below threshold should not be visible in extracellular records, and there should be a number of stimulus spatial phases that evoke no action potentials. We rarely observed this behavior. In fact, thresholds are closely related to large exponents (Tolhurst & Heeger, 1997) and neither is consistent with the counterphase data. Although S-T unoriented cells like that in Fig. 3 displayed little or no response at the null phase, responses at other phases were readily elicited. Thus, an LN model that includes a threshold and exponent does not seem adequate to account for strong direction selectivity in cells with low S-T orientation.

Our data support the conclusions of others (Tolhurst & Dean, 1991; Emerson & Citron, 1989) that dynamic nonlinearities are required to account for robust directional tuning ($DI > 0.8$) in simple cells with very weak S-T orientation ($STI < 0.2$). Studies of higher order receptive-field structure by Emerson and Citron (1989) and Baker and Cynader (1988) have revealed strong dynamic nonlinearities in such cells. In contrast, intracellular recordings of simple cells by Jagadeesh et al. (1993) have not revealed these processes. However, those intracellular recordings were done in layer 4. Our data indicate that dynamic nonlinearities underlying directional tuning may be less prevalent there. It would be interesting to examine layer 6 cells intracellularly for signs of such dynamic nonlinearities.

Implications for circuitry underlying direction selectivity in simple cells

While cells differ in the extent to which they rely on linear and nonlinear mechanisms to create direction selectivity, they all require inputs that are spatially and temporally offset from one another. The spatial disparity is commonly thought to be achieved by partially shifted receptive fields. Sources of the temporal disparities are less clear. Saul and Humphrey (1990, 1992a,b) proposed that LGN cells of the lagged type are responsible for many of the cortical timing delays. Lagged and nonlagged cells provide area 17 with a wide range of input timings, from response phase leads to phase lags. Furthermore, lagged timing signatures are readily observed in simple-cell receptive fields in layers 4B and 5A (Saul & Humphrey, 1992a) but they are rare outside of layer 4. This and

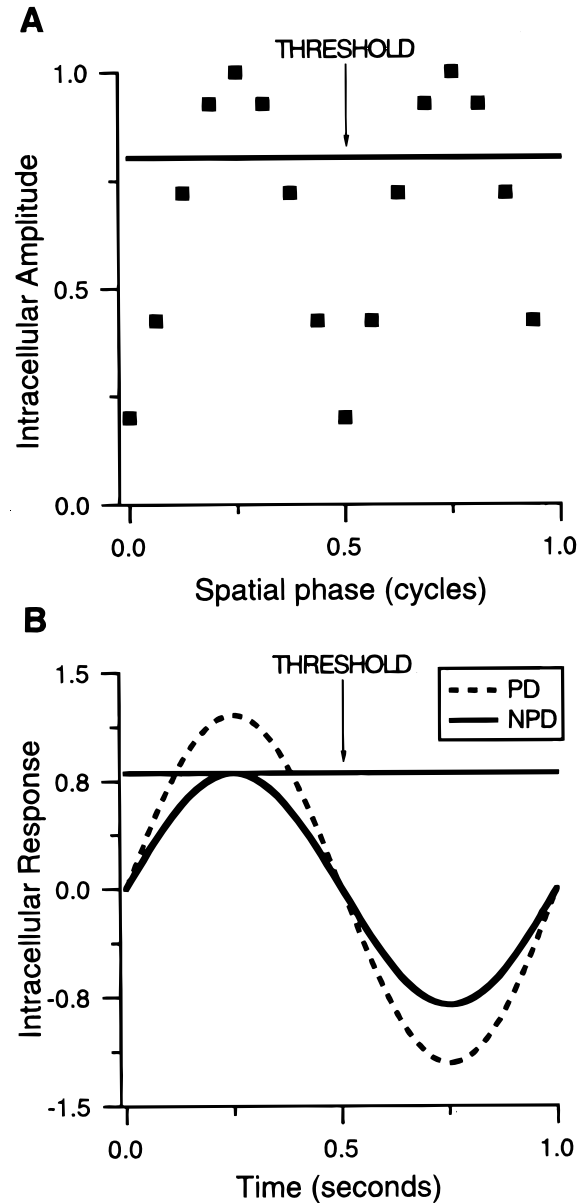


Fig. 12. Hypothetical intracellular responses of a cell with an STI of 0.2. A: Modulation of membrane potential by a counterphasing grating at different spatial phases. B: Expected responses to a grating drifting in the preferred (PD) and nonpreferred (NPD) directions, assuming linear spatiotemporal summation. Only weak direction selectivity ($DI = 0.2$) would be established by the linear mechanism. To produce complete direction selectivity in the cell's spiking behavior would require a very high and finely tuned threshold (horizontal line). However, the high threshold should suppress action potentials at a number of spatial phases when testing with a counterphasing grating (A).

other evidence summarized previously (Humphrey & Weller, 1988; Saul & Humphrey, 1992a) indicates that lagged axons terminate mainly in lower layer 4. Nonlagged timings have a wider laminar distribution that includes all of layers 4 and 6, which is congruent with the known terminations of nonlagged axons (Humphrey et al., 1985; Saul & Humphrey, 1992a).

We suggest that these patterns of geniculocortical inputs underlie some of the laminar differences in S-T orientation. Lagged and nonlagged afferents could provide the range of timings that

underlie many of the space-time well-oriented receptive fields in layers 4B and 5A, and to some extent 4A. With regard to the latter, cells in layer 4A with the strongest S-T orientation were generally recorded in the lower half of the sublayer, where they would be in a position to sample lagged inputs. However, cells with little S-T orientation were also recorded in lower layer 4A. These differences in S-T structure might reflect the relative convergence of lagged and/or nonlagged afferents on different cells. The absence of receptive fields in layer 6 with even moderate S-T orientation may reflect an absence of direct lagged input.

The differences we have observed may also reflect laminar variations in intracortical circuits. For example, complex cells are more common in upper and lower cortical layers than in layer 4 (Gilbert, 1977). Evidence exists for complex-to-simple cell interactions (Hammond & MacKay, 1981; Ghose et al., 1994). It is plausible that simple cells in layer 6 receive more input from complex cells than do most layer 4 cells. The two cell classes display similar directional tuning (Saul & Humphrey, 1992b) but complex cells lack first-order S-T oriented receptive fields. Their direction selectivity is correlated with second-order S-T structure (Emerson et al., 1987). Input from complex cells might therefore confer on layer 6 simple cells a direction selectivity that is not dependent on first-order structure, as observed here. The effect of such input could be to facilitate and inhibit, respectively, responses to the preferred and nonpreferred directions of motion (Emerson & Gerstein, 1977; Goodwin et al., 1975). Simple cells with S-T un-oriented receptive fields in layer 4A and the 3-4 border may be similarly influenced by complex cells in lower layer 3 or by the few complex cells within layer 4.

Other intracortical circuits may dominate in simple cells with S-T oriented receptive fields. We recently showed (Murthy et al., 1995) that the reduction of direction selectivity in simple cells that results from antagonizing GABA_A-mediated inhibition (Sillito, 1984) is accompanied by a reduction in the S-T orientation of the receptive field. Thus, inhibition affects direction selectivity in S-T oriented simple cells by accentuating the S-T orientation of the receptive field without affecting stimulus-induced response modulations that are a hallmark of simple cells. This implies that the inhibitory input comes primarily from other simple cells.

Conclusions

Taken together our observations on S-T receptive-field structure and direction selectivity indicate that an LN model is consistent with the behavior of most cells in layer 4. This implies that linear summation of geniculocortical and intracortical signals with different response timings, followed by relatively simple cortical processes that act as static nonlinearities, underlie direction selectivity in most layer 4 cells. In contrast, the LN model fails for layer 6 cells, and a few cells in layer 4. First-order S-T receptive-field structure plays a less prominent role and circuits that underlie more dynamic nonlinear processing are more important there. Future experimental and modeling studies should be cognizant of these laminar variations.

Acknowledgments

We are grateful to Paul Baker for computer programming, Mark Kieler for electronics support, and Kaiqi Sun for assistance during some of the recordings. This work was supported by National Eye Institute Grants EY06459 (A.L.H.) and EY10826 (A.B.S.), and a Core Grant for Vision Research (EY08098) to the Eye and Ear Institute of Pittsburgh.

References

- ADELSON, E.H. & BERGEN, J.R. (1985). Spatiotemporal energy models for the perception of motion. *Journal of the Optical Society of America A* **2**, 284–299.
- ALBRECHT, D.G. & GEISLER, W.S. (1991). Motion selectivity and the contrast-response function of simple cells in the visual cortex. *Visual Neuroscience* **7**, 531–546.
- ALBRECHT, D.G. & HAMILTON, D.B. (1982). Striate cortex of monkey and cat: Contrast response function. *Journal of Neurophysiology* **48**, 217–237.
- BAKER, C.L., JR. (1994). Space-time separability of direction selectivity in visual cortex neurons. *Investigative Ophthalmology and Visual Science (Suppl.)* **35**, S469.
- BAKER, C.L., JR. & BOULTON, J.C. (1994). Neurobiological mechanisms of cortical direction selectivity. In *Computational Vision Based on Neurobiology*, SPIE Proceedings, 2054, ed. LAWTON, T.B., pp. 104–123. Bellingham, Washington: SPIE.
- BAKER, C.L., JR. & CYNADER, M.A. (1988). Space-time separability of direction selectivity in cat striate cortex neurons. *Vision Research* **28**, 239–246.
- DEANGELIS, G.C., OHZAWA, I. & FREEMAN, R.D. (1993a). Spatiotemporal organization of simple-cell receptive fields in the cat's striate cortex. I. General characteristics and postnatal development. *Journal of Neurophysiology* **69**, 1091–1117.
- DEANGELIS, G.C., OHZAWA, I. & FREEMAN, R.D. (1993b). Spatiotemporal organization of simple-cell receptive fields in the cat's striate cortex. II. Linearity of temporal and spatial summation. *Journal of Neurophysiology* **69**, 1118–1135.
- EMERSON, R.C. & CITRON, M.C. (1989). Linear and nonlinear mechanisms of motion in single neurons of the cat's visual cortex. In *Proceedings of the IEE International Conference on Systems, Man and Cybernetics*, ed. KLEINMAN, D.L., pp. 448–453. Cambridge, Massachusetts: IEEE.
- EMERSON, R.C. & CITRON, M.C. (1992). Linear and nonlinear mechanisms of motion selectivity in simple cells of the cat's striate cortex. In *Non-linear Vision Determinants of Neural Receptive Fields, Function and Networks*, ed. PINTER, R.B. & NABET, B., pp. 75–89. Boca Raton, Florida: CRC Press.
- EMERSON, R.C. & GERSTEIN, G.L. (1977). Simple striate neurons in the cat. II. Mechanisms underlying directional asymmetry and directional selectivity. *Journal of Neurophysiology* **40**, 136–155.
- EMERSON, R.C., CITRON, M.C., VAUGHN, W.J. & KLEIN, S.A. (1987). Nonlinear directionally selective subunits in complex cells of cat striate cortex. *Journal of Neurophysiology* **58**, 33–65.
- GHOSE, G.M., OHZAWA, I. & FREEMAN, R.D. (1994). Receptive-field maps of correlated discharge between pairs of neurons in the cat's visual cortex. *Journal of Neurophysiology* **71**, 330–346.
- GILBERT, C.D. (1977). Laminar differences in receptive field properties of cells in cat primary visual cortex. *Journal of Physiology (London)* **268**, 391–421.
- GOODWIN, A.W., HENRY, G.H. & BISHOP, P.O. (1975). Direction selectivity of simple striate cells: Properties and mechanisms. *Journal of Neurophysiology* **38**, 1500–1523.
- HAMMOND, P. & MACKAY, D.M. (1981). Modulatory influences of moving textured backgrounds on responsiveness of simple cells in feline striate cortex. *Journal of Physiology (London)* **319**, 431–442.
- HEEGER, D.J. (1993). Modeling simple-cell direction selectivity with normalized, half-squared, linear operators. *Journal of Neurophysiology* **70**, 1885–1898.
- HUBEL, D.H. & WIESEL, T.N. (1962). Receptive fields, binocular interaction and functional architecture in the cat's visual cortex. *Journal of Physiology (London)* **160**, 106–154.
- HUMPHREY, A.L. & WELLER, R.E. (1988). Functionally distinct groups of X-cells in the lateral geniculate nucleus of the cat. *Journal of Comparative Neurology* **268**, 429–447.
- HUMPHREY, A.L., SUR, M., UHLRICH, D.J. & SHERMAN, S.M. (1985). Projection patterns of individual X- and Y-cells axons from the lateral geniculate nucleus to cortical area 17 in the cat. *Journal of Comparative Neurology* **233**, 159–189.
- JAGADEESH, B., WHEAT, H.S. & FERSTER, D. (1993). Linearity of summation of synaptic potentials underlying direction selectivity in simple cells of the cat visual cortex. *Science* **262**, 1901–1904.
- MCLEAN, J. & PALMER, L.A. (1989). Contribution of linear spatiotemporal receptive field structure to velocity selectivity of simple cells in area 17 of cat. *Vision Research* **29**, 675–679.

- MCLEAN, J., RAAB, S. & PALMER, L.A. (1994). Contribution of linear mechanisms to the specification of local motion by simple cells in areas 17 and 18 of the cat. *Visual Neuroscience* **11**, 271–294.
- MOVSHON, J.A., THOMPSON, I.D. & TOLHURST, D.J. (1978). Spatial summation in the receptive fields of simple cells in the cat's striate cortex. *Journal of Physiology* (London) **283**, 53–77.
- MURTHY, A.N., SAUL, A.B. & HUMPHREY, A.L. (1997). Laminar differences in spatiotemporal structure of simple cell receptive fields in cat area 17. *Investigative Ophthalmology and Visual Science* (Suppl.) **38**, S623.
- MURTHY, A.N., SUN, K.-Q. & HUMPHREY, A.L. (1995). A role for GABA_A-mediated inhibition in generating the spatiotemporal structure of simple cell receptive fields. *Society for Neuroscience Abstracts* **21**, 1648.
- O'LEARY, J.L. (1941). Structure of the area striata of the cat. *Journal of Comparative Neurology* **75**, 131–164.
- REID, R.C., SOODAK, R.E. & SHAPLEY, R.M. (1987). Linear mechanisms of directional selectivity in simple cells of cat striate cortex. *Proceedings of the National Academy of Sciences of the U.S.A.* **84**, 8740–8744.
- REID, R.C., SOODAK, R.E. & SHAPLEY, R.M. (1991). Directional selectivity and spatiotemporal structure of receptive fields of simple cells in cat striate cortex. *Journal of Neurophysiology* **66**, 505–529.
- SAUL, A.B. & HUMPHREY, A.L. (1990). Spatial and temporal response properties of lagged and non-lagged cells in the cat lateral geniculate nucleus. *Journal of Neurophysiology* **6**, 206–224.
- SAUL, A.B. & HUMPHREY, A.L. (1992a). Evidence of input from lagged cells in the lateral geniculate nucleus to simple cells in cortical area 17 of the cat. *Journal of Neurophysiology* **68**, 1190–1207.
- SAUL, A.B. & HUMPHREY, A.L. (1992b). Temporal frequency tuning of direction selectivity in cat visual cortex. *Visual Neuroscience* **8**, 365–372.
- SIEGEL, S. (1956). *Nonparametric Statistics for the Behavioral Sciences*. New York: McGraw-Hill.
- SILLITO, A.M. (1984). Functional considerations of the operation of GABAergic inhibitory processes in the visual cortex. In *Cerebral Cortex 2*, ed. JONES, E.G. & PETERS, A., (pp. 91–117). New York: Plenum Press.
- SKOTTUN, B.C., DEVALOIS, R.L., GROSOFF, D.H., MOVSHON, J.A., ALBRECHT, D.G. & BONDS, A.B. (1991). Classifying simple and complex cells on the basis of response modulation. *Vision Research* **31**, 1079–1086.
- TOLHURST, D.J. & DEAN, A.F. (1987). Spatial summation by simple cells in the striate cortex of the cat. *Experimental Brain Research* **66**, 607–620.
- TOLHURST, D.J. & DEAN, A.F. (1991). Evaluation of a linear model of directional selectivity in simple cells of the cat's striate cortex. *Visual Neuroscience* **6**, 421–428.
- TOLHURST, D.J. & HEEGER, D.J. (1997). Comparison of contrast-normalization and threshold models of responses of simple cells in cat striate cortex. *Visual Neuroscience* **14**, 293–309.
- WATSON, A.B. & AHUMADA, A.J., JR. (1985). Model of human visual-motion sensing. *Journal of the Optical Society of America A* **2**, 322–341.

Appendix

In this section, we describe the fitting procedure used to make predictions of direction selectivity from response phase data generated from counterphasing gratings. This is done in the framework of a linear spatiotemporal quadrature model (Adelson & Bergen, 1985; Watson & Ahumada, 1985). Here, the output of a neuron is the linear sum of two subunits that are a quarter cycle apart in space and time. For simplicity, the first unit's spatial phase ψ and temporal phase φ are set to 0 cycles. Corresponding phase values for the second unit are each 0.25 cycles. We let the gain of one subunit be fixed at unity and that of the other be a constant, G , with a value between 0 and 1. We show that in a linear system the relative magnitude G of the subunits determines the degree of direction selectivity. The response of each subunit to a drifting sine-wave grating is

$$R_1\{\cos[2\pi(kx \pm \omega t)]\} = \cos(2\pi\omega t) \quad (\text{A1})$$

and

$$R_2\{\cos[2\pi(kx \pm \omega t)]\} = G \cos[2\pi(\omega t + \psi \pm \varphi)] \quad (\text{A2})$$

where $R\{S(x,t)\}$ is the response to stimulus $S(x,t)$, in this case a drifting grating. For simplicity, we omit the luminance terms; ω and k are the temporal and spatial frequencies. The \pm before the temporal term signifies the direction of motion. Substituting 0.25 for ψ and φ in eqn. (A2) and summing the response of both subunits in each direction of motion, we get

$$R_{\text{NPD}} = \cos(2\pi\omega t) + G \cos[2\pi(\omega t + 0.5)] \quad (\text{A3})$$

$$= (1 - G)\cos(2\pi\omega t)$$

$$R_{\text{PD}} = \cos(2\pi\omega t) + G \cos(2\pi\omega t) \quad (\text{A4})$$

$$= (1 + G)\cos(2\pi\omega t)$$

where R_{NPD} and R_{PD} are the outputs of the cell in the preferred and non-preferred directions, respectively, their amplitudes being $(1 - G)$ and $(1 + G)$. Substituting these values in eqn. (1),

$$DI = [(1 + G) - (1 - G)] / [(1 + G) + (1 - G)] \quad (\text{A5})$$

$$\therefore DI = G \quad (\text{A6})$$

The relative gain of the second subunit determines the degree of direction selectivity.

Now consider the response to a counterphasing grating at some spatial phase ψ . As before, we omit the luminance terms for simplicity.

$$R\{\sin[2\pi(kx + \psi)]\sin(2\pi\omega t)\}$$

$$= \sin(2\pi\psi)\sin(2\pi\omega t) + G\cos(2\pi\psi)\cos(2\pi\omega t) \quad (\text{A7})$$

where, $\sin(2\pi\psi)\sin(2\pi\omega t)$ is the response of the first subunit (R_1) and $G\cos(2\pi\psi)\cos(2\pi\omega t)$ is the response of the second subunit (R_2) which is in spatial and temporal quadrature. Again, the constant, G , is the relative gain of the second subunit. The coefficients $\sin(2\pi\psi)$ and $G\cos(2\pi\psi)$ in eqn. (A7) are the amplitudes of each subunit. Their ratio determines the temporal phase φ , and the square root of their summed squares determines the amplitude A , of the response:

$$\varphi(\psi) = \frac{1}{2\pi} \tan^{-1} \left(\frac{\tan(2\pi\psi)}{G} \right) \quad (\text{A8})$$

and

$$A(\psi) = A_{\text{max}}[\sin^2(2\pi\psi) + G^2 \cos^2(2\pi\psi)]^{1/2} \quad (\text{A9})$$

Since actual receptive fields have arbitrary spatial and temporal phases with respect to the counterphasing grating, we have to include two additional parameters in eqns. (A8) and (A9). Substituting STI for G , we get

$$\varphi(\psi) = \varphi_0 + \frac{1}{2\pi} \tan^{-1} \left(\frac{\tan[2\pi(\psi - \psi_0)]}{STI} \right) \quad (\text{A10})$$

and

$$A(\psi) = A_{\text{max}}\{\sin^2[2\pi(\psi - \psi_0)] + STI^2 \cos^2[2\pi(\psi - \psi_0)]\}^{1/2} \quad (\text{A11})$$

where φ_0 provides the necessary temporal offset and ψ_0 the spatial offset. These two parameters, along with STI , are free to vary. Eqn. (A10) is fit to the temporal phase *versus* spatial phase data in each half-cycle. Since STI equals DI [see eqn. (A6)], it yields a predicted direction selectivity based on the temporal receptive-field structure. It is important to note that this

measure is independent of response amplitudes and hence not affected by the presence of static nonlinearities. To get a more intuitive sense of what the *STI* parameter in the fit corresponds to, we derive analytically the relation between the slope ($d\varphi/d\psi$) and *STI*.

Taking the derivative with respect to ψ on either side of eqn. (A10) with φ_0 and $\psi_0 = 0$ gives

$$\frac{d\varphi}{d\psi} = \frac{STI}{STI^2 \cos^2 2\pi\psi + \sin^2 2\pi\psi} \quad (\text{A12})$$

At $\psi = 0.25$ or 0.75 , we get

$$(d\varphi/d\psi)_{\psi=0.25,0.75} = STI \quad (\text{A13})$$

i.e. in a linear neuron the slope of the temporal phase versus spatial phase plot at $\psi = 0.25$ or 0.75 cycles is the *STI* and is equal to the cell's linear direction selectivity. It also corresponds to the minimum of the function in eqn. (A12). This can be more easily visualized by observing the fits for layer 4B cells in Fig. 5. The gradients are the smallest at spatial phases of 0.25 and 0.75 . Although not shown, they are also characterized by having the greatest response amplitudes because they lie at the optimal spatial phases [see eqn. (A9)].

A related measure of S-T orientation that has been used in a previous study (Albrecht & Geisler, 1991) involves estimating the slope of the best-fit line to the response phase *versus* spatial phase data. Such a measure has two drawbacks. First, the response phase data do not describe a line except for the extreme cases (i.e. when *STI* is either 0 or 1). This is true in a strictly linear model and it is true for most of the data observed. Second, being the average as opposed to the minimum slope, it overestimates the linear *DI*.